

Document downloaded from:

<http://hdl.handle.net/10251/37356>

This paper must be cited as:

Candel Busquets, I.; Aznar Gimeno, E.; Mondragón Martínez, L.; Martínez Mañez, R.; Sancenón Galarza, F.; Marcos Martínez, MD.; Amoros Del Toro, PJ... (2012). Amidase-responsive controlled release of antitumoral drug into intracellular media using gluconamide-capped mesoporous silica nanoparticles. *Nanoscale*. 4(22):7237-7245. doi:10.1039/c2nr32062b.



The final publication is available at

<http://dx.doi.org/10.1039/c2nr32062b>

Copyright Royal Society of Chemistry

Cite this: DOI: 10.1039/c0xx00000x

www.rsc.org/xxxxxx

PAPER

## Antitumoral drug amidase-responsive controlled release on intracellular media using gluconamide-capped mesoporous silica nanoparticles.

Inmaculada Candel,<sup>a,c</sup> Elena Aznar,<sup>c,a</sup> Laura Mondragón,<sup>a,b,c</sup> **Cristina de la Torre,<sup>a,c</sup>** Ramón Martínez-Mañez,<sup>a,b,c,\*</sup> Félix Sancenón,<sup>a,b,c</sup> M. Dolores Marcos,<sup>a,b,c</sup> Pedro Amorós,<sup>e</sup> Carmen Guillem,<sup>e</sup> Enrique Pérez-Payá,<sup>f,g</sup> Ana Costero,<sup>a,d</sup> Salvador Gil,<sup>a,d</sup> Margarita Parra<sup>a,d</sup>

Received (in XXX, XXX) Xth XXXXXXXXX 20XX, Accepted Xth XXXXXXXXX 20XX

DOI: 10.1039/b000000x

TMCM-41 silica nanoparticles were used as inorganic scaffolding to prepare a nanoscopic-capped hybrid material **S1**, which was able to release an entrapped cargo in the presence of certain enzymes, whereas in the absence of enzyme, a zero release system was obtained. **S1** was prepared by loading nanoparticles with safranin O dye and was then capped with a gluconamide derivative. In the absence of enzyme, the release of the dye from the aqueous suspensions of **S1** was inhibited as a result of the steric hindrance imposed by the bulky gluconamide derivative, the polymerized gluconamide layer and the formation of a dense hydrogen-bonded network around the pore outlets. Upon the addition of amidase and pronase enzymes, delivery of safranin O dye was observed due to the enzymatic hydrolysis of the amide bond in the anchored gluconamide derivative. **S1** nanoparticles were not toxic for cells, as demonstrated by cell viability assays using HeLa and MCF-7 cell lines, and were associated with lysosomes, as shown by confocal microscopy. Finally, the **S1-CPT** material loaded with the cytotoxic drug camptothecin and capped with the gluconamide derivative was prepared. The HeLa cells treated with **S1-CPT** underwent cell death as a result of material internalization, and of the subsequent cellular enzyme-mediated hydrolysis and aperture of the molecular gate, which induced the release of the camptothecin cargo.

### INTRODUCTION

The preparation of hybrid functional materials in an attempt to mimic objects that perform active tasks in living organisms is a fertile multidisciplinary research area<sup>1</sup>. Nature uses simple molecules (amino acids, saccharides, nucleobases and certain inorganic compounds) to design functional structures (channels, pumps, gates) of a nanometric size. Chemists, inspired by these biological systems, have started to develop nanometric functional materials that work similarly to these complex structures in living organisms<sup>2</sup>.

One of the most appealing concepts in nature is related with channels that act as gates and control mass transport on command. Inspired by this concept, researchers have recently been involved in the design of “molecular gates”<sup>3</sup>. A molecular gate can be defined as a nanoscopic system in which mass transport (or delivery) can be triggered by a target external stimulus, which is able to control the state of the gate (closed or open) at will. In general, an abiotic gated material is composed of two subunits: (i) a suitable inorganic support and (ii) certain organic molecules, usually grafted on the external surface, which are the responsible for mass transport/delivery control.

In most prepared gated materials, silica mesoporous supports of the MCM-41 family have been used as inorganic scaffolds.

This is due to the special properties of these materials, such as large load capacity, biocompatibility, high thermal stability, homogeneous porosity, inertness, and tunable pore sizes with a diameter of ca. 2-10 nm. In addition, the existence of well-known surface functionalization procedures makes these scaffoldings suitable to develop molecular gated systems.

Since the first example of a gate-like ensemble based on mesoporous materials was described by Fujiwara et al.,<sup>4</sup> many different molecular gated organic-inorganic hybrid materials using a wide range of different chemistries have been reported.<sup>5</sup> Following this pioneering work, several research groups have demonstrated that it is possible to design gated materials capable of achieving “zero release”, which can be fully opened by applying certain external stimuli. Both physical and chemical triggers, such as pH,<sup>6</sup> temperature,<sup>7</sup> redox potential,<sup>8</sup> light<sup>9</sup> or reaction with chemical species,<sup>10</sup> have been reported. Most systems have been designed for drug delivery applications, although sensing protocols using molecular gated supports have also been described<sup>10b,c,d</sup>.

Despite the fact that molecular gated devices have been studied over the last few years, the use of silica mesoporous gated-like devices involving biomolecules like caps or stimuli to deliver the cargo has not been fully explored. For instance, a few examples using specific drugs as cargo,<sup>11</sup> biomolecules as capping agent,<sup>12</sup>

or enzymes as external stimuli<sup>13</sup> have been described. In particular, very few examples using enzymes have been reported and most cases have focused on peptide-capped nanocontainers capable of releasing their cargo in the presence of the appropriate peptidase.<sup>13e,f</sup> The development of enzyme-responsive bio-gated mesoporous silica nanoparticles is appealing taking into account the wide range of available enzymes able to selectively catalyse a large number of different chemical reactions. In particular, the possibility of prepare tailor-made sequences, that may provide fine selectivity in the design of advanced gate-opening devices, opens new perspectives of applicability for drug delivery systems using mesoporous nanoscopic gated systems.

The use of molecular gated devices based on mesoporous silica nanoparticles as drug containers offers very promising applications in the field of medicine as they would allow the controlled and specific deliver of the drug in the target organ, thus avoiding degradation of the drug by other physiological agents.<sup>14</sup> The application of these concepts in antitumoral medicine has become an area of great interest.<sup>15</sup> Thus, the research community is making great efforts to develop new, innovative mass transport devices capable of delivering anticancer drugs on tumour cells.

By bearing in mind the fact that there are very few examples of gated materials based on the enzymatic hydrolysis of capping groups and taking into account the potential applications of such systems to develop nanodevices showing a “zero release” before the presence of target enzymes, we report herein the design of new and simple capped nanoparticles displaying enzyme-induced delivery. Mesoporous silica nanoparticles were used as inorganic scaffolding while their external surface was functionalized with a gluconamide derivative capable of being hydrolyzed in the presence of the corresponding specific amidases both *in vitro* and on intracellular media. Materials’ efficiency was tested using dye molecules as the cargo to prove both the delivery profiles and the non toxicity of the silica nanoparticles in cells. Moreover, camptothecin- (CPT) loaded nanoparticles were proved to cause cell death in several cancer cell lines.

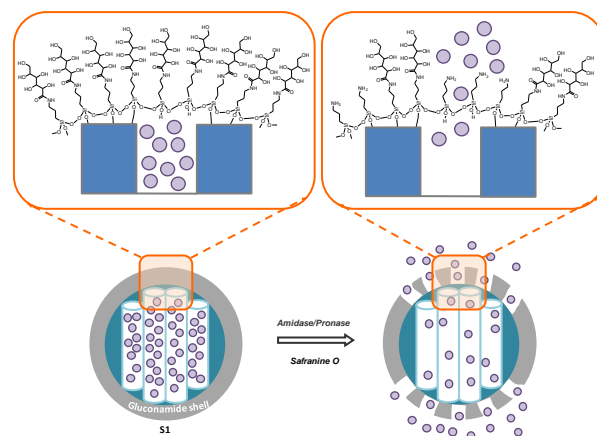
## RESULTS AND DISCUSSION

### Design and synthesis of gated materials

Application of supramolecular chemistry principles to design gate-like ensembles based on mesoporous scaffoldings allows the development of nanoscopic devices for mass transport and controlled release applications. As stated in the Introduction, most developed gated materials employ molecular/supramolecular interactions for the fine control of cargo delivery. In contrast, relatively few examples use biomolecules for capping or uncapping protocols. Following our interest in applying biological interactions, as triggered for control delivery, here we paid attention to using enzymes as “biological-keys”.

Our aim was to design biocompatible easy-to-prepare capping systems in order to synthesize simple gated scaffoldings capable of being used efficiently in delivery applications. With this approach, silica mesoporous MCM-41 nanoparticles were selected as inorganic scaffolds. Scheme 1 shows the proposed enzyme-driven gate-opening mechanism for the new gated

material **S1**. In order to prepare the designed material, the pores of the MCM-41-type nanoparticulated scaffolding were loaded with safranin O. Then the external surface was functionalized with *N*-(3-triethoxysilylpropyl)gluconamide to yield the final hybrid material **S1**. This organic compound has been selected by bearing in mind the presence of an amide hydrolysable group and five hydroxyl groups, which were expected to result in a dense hydrogen-bonded network around the pore outlets, which should avoid cargo delivery. In the presence of the appropriate amidase, the amide bond is hydrolyzed with the subsequent reduction in size of the attached capping molecule and, consequently, the delivery of the cargo. In order to completely block the drug inside the mesopores in the absence of amidase (to favor a selective drug release), we used a higher proportion of *N*-(3-triethoxysilylpropyl)gluconamide if compared to previous works of our group (*vide infra*). Under these conditions, and together with the direct silica surface functionalization (by the interaction of the silanol groups with the triethoxy moieties of the silane), a certain polymerization of the silane on the silica surface was expected (in this last case, by using a limited number of silanol groups to maintain the interaction with the support). Thus, this strategy guarantees the formation of a thicker shell around the mesoporous silica nanoparticles. However, regardless of the nature of the incorporated silanes (directly functionalized or polymerized), the enzyme was expected to be able to cut the organic arms inducing the drug release.



**Scheme 1** Schematic representation of the synthesis procedure and the gate-opening mechanism of **S1** in the presence of the appropriate enzyme.

The silica nanoparticulated material (a calcined MCM-41-like solid) was prepared by following well-known procedures using TEOS as the hydrolysable inorganic precursor and the surfactant hexadecyltrimethylammonium bromide (CTABr) as the porogen species.<sup>16</sup> Moreover *N*-(3-triethoxysilylpropyl)gluconamide is a commercially available alkoxy silane derivative, which was selected and used as the molecular gate.

In order to ensure the correct functionality of the final hybrid material, we followed a two-step synthetic procedure which we and others have previously used to prepare gated structures containing a loaded cargo on the pores and suitable switchable ensembles on the pore outlets.<sup>6e</sup> In the first step, the efficient loading of pores was achieved by stirring a highly concentrated Safranin O solution in the presence of the mesoporous

nanoparticles. Then in a second step, the gluconamide derivative was added to the same mixture to functionalize the external surface of the siliceous material. Following this protocol, the anchoring reaction of *N*-(3-triethoxysilylpropyl)gluconamide occurred on the nanoparticles containing pores filled with safranin O in a suspension which still contained a high concentration of the dye, thus inhibiting dye diffusion from the inner pores to the bulk solution and, at the same time, hampering as much as possible the entrance of *N*-(3-triethoxysilylpropyl)gluconamide into the porous network.

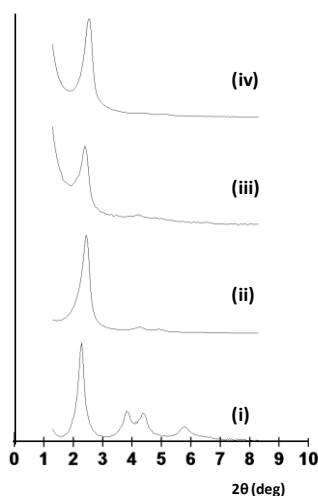


**Fig. 1** XRD Patterns for the nanoparticulated MCM-41 as-synthesized (i), calcined MCM-41 nanoparticles (ii), **S1** (iii) and **S1-CPT** (iv).

Following this protocol, the final **S1** material should contain the gluconamide derivative, mainly as a shell on the external surface (*vide infra* for a more detailed comment), whereas safranin O should be located inside the mesopores. Finally, the violet/pinkish solid **S1** was filtered, washed with water and dried at 40°C for 12 h.

A second solid, **S1-CPT**, was prepared following the same procedure as cited above. In this case, mesopores were filled with the anticancer agent camptothecin, and the uptake was performed in acetonitrile-ethanol mixtures to favor drug dissolution. Then, *N*-(3-triethoxysilylpropyl)gluconamide was added to the suspension and the final material was isolated by filtration, washed with chloroform-methanol 3:4 v/v and dried at vacuum for 1 h.

### Characterization of solids

The prepared material **S1** was characterized by standard techniques. Figure 1 shows the powder X-ray diffraction (XRD) patterns of solids MCM-41 as synthesized, MCM-41 calcined, **S1** and **S1-CPT**. The XRD of the mesoporous MCM-41 material as-synthesized (Figure 1, curve i) displayed the expected four peaks of a hexagonal ordered array indexed as (100), (110), (200), and (210) Bragg reflections. From the XRD data, an  $a_0$  cell parameter of 41 Å ( $d_{100}$  spacing of 36.05 Å) was calculated. In curve ii, corresponding to the MCM-41 calcined sample, a significant shift of the (100) reflection in the XRD is clearly observed. This

displacement, together with the broadening of the (110) and (200) reflections, corresponds to an approximate cell contraction of *ca.* 6-8 Å due to the condensation of silanols groups in the calcination step. Figure 1 also depicts the XRD patterns for solids **S1** and **S1-CPT**. For these materials, reflections (110) and (200) were lost, most likely due to a reduced contrast as the result of the loading and functionalization process. Yet the presence of the  $d_{100}$  peak in the XRD patterns in both **S1** and **S1-CPT** suggested that the pore loading (with Safranin O dye or with the camptothecin drug) and functionalisation process did not modify the mesoporous MCM-41 scaffolding.

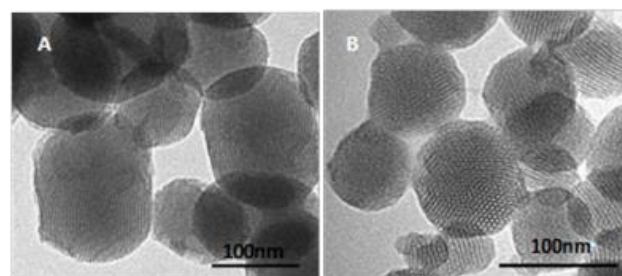


**Fig. 2** Representative Transmission Electron Microscopy (TEM) image of the calcined MCM-41 nanoparticles (A) and the loaded and functionalized mesoporous silica nanoparticles (**S1**) (B).

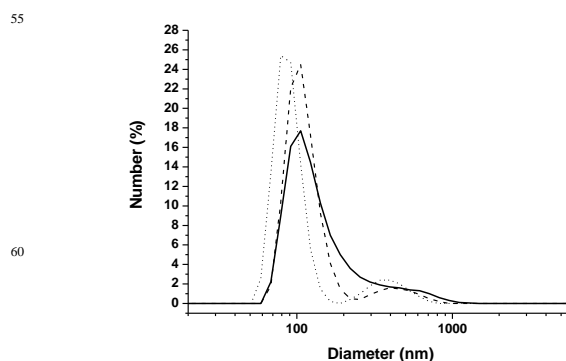


**Fig. 3** Statistical representation of particle size obtained by DLS (Dynamic Light Scattering) studies. The average size of nanoparticles of calcined MSN (straight), **S1** (dash) and **S1-CPT** (dot) was found to be *ca.* 100 nm.

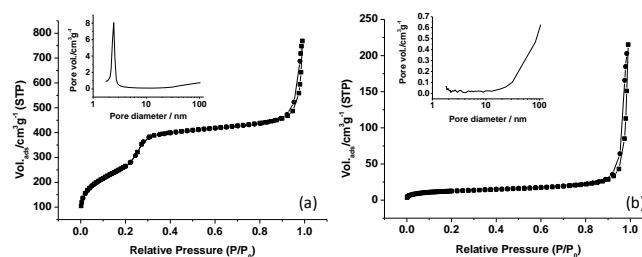


**Fig. 4** Nitrogen adsorption-desorption isotherms for (a) the MCM-41 mesoporous nanoparticles (b) **S1**. Insets: Pore size distribution of each material.

Preservation of the mesoporous structure in the final functionalized solid **S1** was also confirmed by the Transmission Microscopy (TEM) images. Figure 2 shows the morphology of

the prepared mesoporous materials. MCM-41 scaffolding was obtained as spherical particles showing a mean diameter of 80-100 nm. From the images, it is apparent that the loaded and functionalized derivative **S1** maintains the initial MCM-41 matrix morphology. A similar result was obtained for **S1-CPT** (data not shown). In all the samples, the characteristic channels of a mesoporous matrix were observed as alternate black and white lines.

**Table 1** BET-specific surface values, pore volumes and pore sizes (associated with intraparticle mesopores) calculated from the N<sub>2</sub> adsorption-desorption isotherms for each material.

	Mesopore Size (nm)	Mesopore Volume (cm <sup>3</sup> g <sup>-1</sup> )	Large pore Volume (cm <sup>3</sup> g <sup>-1</sup> )	BET surface area (m <sup>2</sup> g <sup>-1</sup> )
MCM-41	2.40	0.71	0.39	963.3
<b>S1</b>	-	< 0.03	0.23	45.6

**Table 2.** Contents of the alcoxysilane derivative and cargo found on **S1** and **S1-CPT**

	Alcoxysilane derivative (mmol/g SiO <sub>2</sub> )	Safranin O Content (mmol/g SiO <sub>2</sub> )	CPT content (mmol/g SiO <sub>2</sub> )
<b>S1</b>	3.47	0.25	-
<b>S1-CPT</b>	1.35	-	0.27

Further DLS (Dynamic Light Scattering) studies showed particles with a mean diameter of 100 nm. The studies also shown that the size of the nanoparticles was not modified throughout the loading and functionalization processes (figure 3). Signals at ca. 500 nm suggested that a small proportion of the nanoparticles were aggregated.

The N<sub>2</sub> adsorption-desorption isotherms of the nonparticulated MCM-41 calcined material are shown in Figure 4. A typical curve for this mesoporous support, consisting of an adsorption step at an intermediate  $P/P_0$  value (0.1-0.3), is observed. This curve matches a type IV isotherm in which the observed step deals with nitrogen condensation inside the mesopores. The narrow BJH pore distribution and the absence of a hysteresis loop in this interval suggest the existence of uniform cylindrical mesopores (pore diameter of 2.40 nm and pore volume of 0.71 cm<sup>3</sup> g<sup>-1</sup> calculated by using the BJH model on the adsorption branch of the isotherm). Application of the BET model resulted in a value of 963.3 m<sup>2</sup> g<sup>-1</sup> for the total specific surface. From the XRD, porosimetry and TEM studies, the  $a_0$  cell parameter (4.1 nm), the pore diameter (2.40 nm), and the wall thickness value of 1.7 nm were calculated. In addition to this adsorption step, a second feature is observed in the isotherm at a high relative pressure ( $P/P_0$  0.8), which corresponds to the filling of the large voids among the particles (0.48 cm<sup>3</sup> g<sup>-1</sup> calculated by the BJH model) and must be considered a textural-like porosity.

In this case, the curves show a characteristic H1 hysteresis loop and a wide pore size distribution. The N<sub>2</sub> adsorption-desorption isotherm of **S1** is typical of mesoporous systems with practically filled mesopores (see Figure 4). Consequently, relatively low N<sub>2</sub> adsorbed volume (BJH mesopore volume (0.03 cm<sup>3</sup> g<sup>-1</sup>) and surface area (45.6 m<sup>2</sup> g<sup>-1</sup>) values were calculated, thus indicating effective pore blocking and the subsequent absence of appreciable mesoporosity. BET-specific surface values, mesopore volumes and mesopore sizes were calculated from the N<sub>2</sub> adsorption-desorption isotherms for MCM-41 and **S1** and are listed in Table 1.

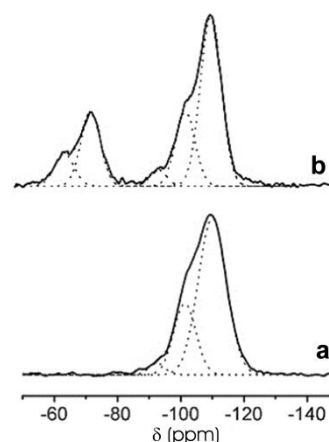


**Fig.5** <sup>29</sup>Si-NMR of the MCM-41 as synthesized (a) and **S1** (b) showing the evolution of the Q<sup>2</sup>+Q<sup>3</sup> and T sites through the loading and functionalization process.

The contents of *N*-(3-triethoxysilylpropyl)gluconamide and Safranin O dye or camptothecin in solid **S1** and solid **S1-CPT** respectively were determined by elemental and thermogravimetric analyses and are shown in Table 2. The amount of CPT present in **S1-CPT** before the functionalization with the gluconamide groups was ca. double of the final content (data not shown). The high content of the organosilane groups incorporated into **S1** indicates that functionalization was not restricted to only direct interactions between silanol groups and the triethoxy moieties of the silanes on the external surface. Then, incorporation of the silanes anchored onto the internal surfaces (mesopore entrances), and even external polymerization, cannot be discarded (according to the experimental conditions used). The capability of the organo-silanes to modify the internal surface of mesopores, even in the case of materials with filled mesopores (with guest species), has been previously described.<sup>17</sup> In fact, effective anchoring of the silanes inside mesopores of up to 8-10 nm deep has been usually observed. Then, besides the external surface of the MCM-41 particles (ca. 70 m<sup>2</sup>/g) (determined from the N<sub>2</sub> adsorption isotherms on the as-synthesized material), an extra surface of ca. 178 m<sup>2</sup>/g of the internal mesopores should be considered as being accessible for the gluconamide containing silanes (this last value has been roughly estimated from the internal surface (963 m<sup>2</sup>/g) by assuming an average particle diameter of 100 nm, and a maximum of 10 nm in deep functionalization, and by also bearing in mind that each mesopore has two entrances). In short for **S1**,

we obtained an average total surface of 248 m<sup>2</sup>/g for organosilane incorporation.

By taking into account that the normal density of the silanol groups in silica materials is *ca.* 6 Si-OH nm<sup>2</sup> and that the gluconamide derivative has three reactive ethoxy groups, the maximum density of the gluconamide groups directly anchored onto hybrid solids should be expected to be *ca.* 2-3 molecules/nm<sup>2</sup>. By assuming our anchoring model and the available 278 m<sup>2</sup>/g surface, only 0.82 mmol of the functional groups could be admitted by our MCM-41. Then, a significant amount of the N-(3-triethoxysilylpropyl)gluconamide groups are necessary incorporated through polymerization around the silica particles to form an organosilane shell. This assembling model is supported by NMR data. The <sup>29</sup>Si NMR spectra of MCM-41 and **S1** are shown in Figure 5. The evolution of the Q<sup>2</sup>+Q<sup>3</sup> sites from 28% (MCM-41) to 23% (**S1**) indicates that most of the silanol groups inside the mesopores remain unaltered. This fact is compatible with our model, where the N-(3-triethoxysilylpropyl)gluconamide groups can be connected on a maximum silica surface of *ca.* 248 m<sup>2</sup>/g. In fact, a maximum estimated percentage of *ca.* 7% of the Q<sup>2</sup>+Q<sup>3</sup> sites is accessible on this surface. Together with this decrease in the silanol groups, the T sites significantly increase (from 0 to 28%) after functionalization. Obviously, this high proportion of T sites is not compatible only with a direct polymerization of silanes on the external silica surface. Therefore, the presence of such a large amount of gluconamide moieties can be associated only with a significant polymerization of the N-(3-triethoxysilylpropyl)gluconamide groups around the silica particles, which require a limited number of silanol groups to preserve the connection with the support. Moreover, this model is in accordance with the relatively low condensation of the organosilane network (T3:T2= 19:9).

### Functional enzyme-driven controlled release

In this section, several experiments were carried out in order to study the enzyme-responsive controlled-release protocol using capped materials in detail. The controlled release behavior of **S1** was studied in aqueous media in the presence of two different enzymes (pronase, a non specific peptidase from *Streptomyces griseus* at pH 8.3; an amidase from *Citrus sinensis* at pH 7.5). The selected pHs are those at which the enzymes presented their optimal activity. In a first experiment, solid **S1** (2.5 mg) was suspended in 25 mL of an aqueous solution (pH 8.3) containing pronase and the final suspension was stirred. The uncapping and subsequent delivery of the dye was easily detected by monitoring the safranin O emission band centered at 580 nm (excitation at 520 nm). As a control experiment, dye release was also measured using suspensions of **S1** under similar conditions, but in the absence of pronase. The difference in dye delivery in both experiments is displayed in Figure 6. Each point in the figure was determined using the above-described protocol, the suspension was filtered at a certain time and the emission of safranin O in the solution was measured. In the absence of the pronase enzyme, a flat baseline was found, indicating that the safranin O cargo remained in the nanoparticles without release. In contrast, in the presence of pronase, delivery of safranin O was observed as increased dye fluorescence in terms of time (see Figure 6). The maximum delivery of safranin O dye from final material **S1**

amounted to 0.28 % in weight was determined by suspending a certain amount of **S1** in water at pH 8.3 containing pronase and by allowing a complete dye delivery for at least 48 h. Under similar conditions, but in the absence of an enzyme, the maximum safranin O dye delivery from **S1** was less than 0.01% in weight. This enzyme-induced release was ascribed to the hydrolysis of the amide bond located in the anchored derivative, which resulted in both the reduced size of the appended groups and the destruction of the dense hydrogen bond network provided by the attached gluconamide.

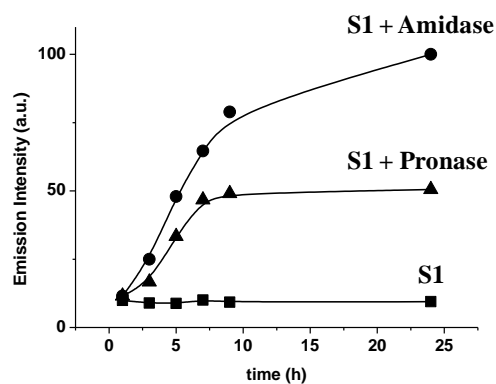


**Fig. 6** Release profiles in the absence and the presence of *Pronase* from *Streptomyces Griseus* and *Peptide Amidase* from *Citrus Sinensis*. The release of Safranin O was monitored via the fluorescence emission band centred at 580 nm ( $\lambda_{exc} = 520\text{nm}$ ).

In spite of the considerable size reduction upon the hydrolysis of the amide bond, the dye release was slow and a constant cargo delivery was observed by at least 10 h. This low delivery rate may be ascribed to the location of the amide bond, which was deep inside the thread and close to the inorganic scaffolding surface. This position of the hydrolysable group hampers fast hydrolysis in the presence of pronase or amidase, and suggests that it is possible to modulate the release kinetics by locating amide moieties in different parts of the molecular threads.

Pronase is a mixture of proteinases that is able to induce the hydrolysis of the amide bond and the release of safranin O to the solution. In order to study the cargo delivery in more detail, some other enzymes were also tested. Figure 6 also displays the delivery profile found in the presence of amidase from *Citrus sinensis* at pH 7.5 using similar experimental conditions to those previously studied in the presence of pronase. Moreover at pH 7.5, and in the absence of an enzyme, a flat curve was found, thus confirming the selective rupture of the amidase bond only in the presence of enzyme. As observed in the figure, greater delivery in this case was obtained when compared with pronase, which is most probably due to the different active concentration of both enzymes. In a final experiment, the cargo delivery from **S1** was also tested in the presence enzyme *Esterase* from *Porcine Liver*; as expected, no delivery was observed under these conditions. During another experiment, it was also verified that the safranin O cargo remained in the **S1** nanoparticles when the solid was in DMEM supplemented with 10% of FCS, which simulates typical cell culture conditions and indicates that no delivery was found using a medium with high salt concentrations.

It should be noted that we previously prepared mesoporous nanoparticles functionalized with gluconamide groups on the external surface. In our previous example, a significant cargo delivery was observed when nanoparticles were suspended in water in the absence of enzymes.<sup>10b,13d</sup> However, as previously explained, a “zero release” was found in this new prepared **S1** material. This different behavior can be explained by the different degree and type of gluconamide functionalization in these solids. Thus, whereas our previous material contained 0.07 g of the gluconamide derivative per g of SiO<sub>2</sub> (mainly anchored directly onto the silica surface), in **S1**, functionalization was larger and the final solid contained 0.81 g of gluconamide/g SiO<sub>2</sub> (combining direct functionalized groups and polymerized ones to form a relatively thick organosilane shell). It is apparent from these data that a simple control of the amount of capping molecule attached to nanoparticles allows the design of systems that either only tune the entrapped cargo delivery rate (our previously reported system) or show a remarkable inhibition of dye delivery (the system reported herein).

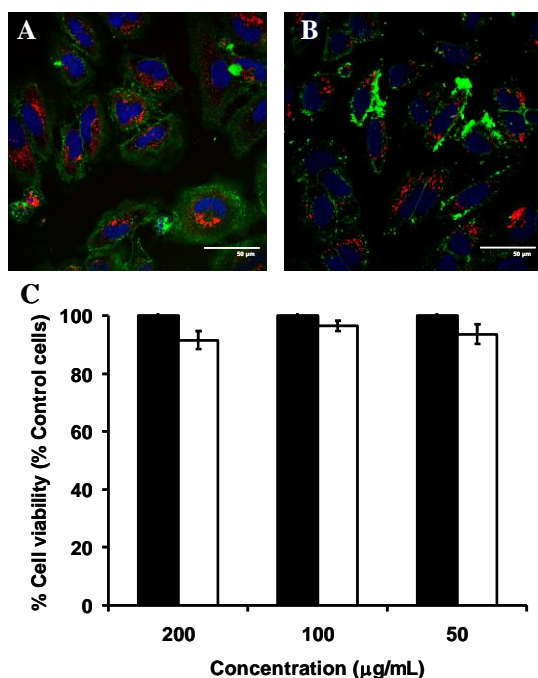


**Fig. 7** **S1** Cellular internalization and WST-1 cell viability assay. HeLa and MCF-7 cells were treated with **S1** at concentrations of 200, 100 and 50 µg/mL for 24 h. Then, the confocal microscopy studies of the **S1** cellular uptake in HeLa (A) and MCF-7 (B) at the 100 µg/mL concentration were performed by Safranin O-**S1**-associated fluorescence (red) in the presence of DNA marker Hoechst 33342 (blue) and plasma membrane marker WGA Alexa Fluor 647 (green). For the cell viability studies, (C) HeLa (black bars) and MCF-7 (white bars) cells were incubated for 24 h with **S1** at the concentrations stated before, while cell viability was quantified by employing the WST-1 reagent. Two independent experiments were performed and the data are represented as (mean ± SE).

### 35 Delivery of Gated Materials in Intracellular Media

Having demonstrated the *in vitro* enzyme-controlled aperture of the gated material, cellular uptake of **S1** and cargo release experiments were carried out. Our main objective was to validate these nanoparticles as drug reservoirs for on command release once inside the cells. For these experiments, two different tumorigenic cell lines, HeLa and MCF-7, were used. Firstly, cell viability studies were done to rule out any toxic effect due to the nanoparticles themselves or to the nature of the molecular gate. Briefly, cells were treated with **S1** for 24 h before adding the WST-1 reagent. This yellow reagent can be reduced by metabolically active cells by mitochondrial enzymes to give a reduced orange soluble product. By measuring absorbance at 450 nm and the subsequent normalization of these measures at 690 nm, the innocuous effect of **S1** on cells was proved at the concentrations tested (see Figure 7). To complement this cell viability assay, confocal microscopy internalization studies were also carried out by taking advantage of Safranin O **S1**-associated fluorescence (see Figures 6A and 6B for further details). In the images obtained, cells were also stained with DNA-associated dye Hoechst 33342 and the plasma membrane marker wheat germ agglutinin Alexa Fluor 647. A dotted pattern associated with **S1** can be observed, which is comparable with that obtained by lysosomes staining, indicating that the possible internalization mechanism of the nanoparticle is endocytosis (Figures 6A and 6B).

Having tested the biocompatibility of the **S1** solid, a new nanoparticulated material containing the chemotherapeutic agent camptothecin (CPT) was synthesized (**S1-CPT**). As stated above, **S1-CPT** was prepared by following a similar procedure to that followed for **S1**, which consists in mesoporous nanoparticles loaded with CPT and capped with the gluconamide derivative. CPT is a quinoline alkaloid employed in the treatment of different cancer types given its ability to inhibit DNA polymerase I, thus disrupting DNA replication processes and inducing cell death. However, its low solubility prevents its application in patients.<sup>18</sup> In this case, HeLa cells were employed to demonstrate the possible cellular internalization of **S1-CPT**, the possible release of the cargo molecule after lysosomal localization and the subsequent uncapping by lysosomal enzymes. Therefore, cells were treated with these new nanoparticles for 48 h at different concentrations before performing the confocal microscopy and flow cytometry analyses. The confocal microscopy results obtained are shown in Figure 8. The cytotoxic effect of **S1-CPT** is clearly noted when compared to MCM-41-treated cells. CPT release induced cell death and detached cells showing membrane blebbing are observed (Figure 8).

For the flow cytometry studies, quantification of CPT-associated cell death was performed by using propidium iodide (PI) and Annexin V (Ann V) markers, which stain dead cells and cells undergoing cell death, respectively. After 48 h of treatment, the **S1-CPT**-treated cells presented an increment in dead cells (ca. 20%) and cells undergoing cell death when compared to the MCM-41-treated cells. This fact proves the release of the cargo molecule inside the cell, this confirming the possible use of **S1** as a drug-carrier of CPT. The main reason behind the relatively low percentage of cell death after 48 h of treatment was most likely due to the relatively low loading of CPT into the mesopores. According to the thermogravimetric and elemental analysis the

**S1-CPT** solid contains 0.27 mmoles CPT per gram of SiO<sub>2</sub> (vide ante). This is a lower value to that found in some other capped mesoporous supports containing CPT (for instance 0.43 mmol of CPT / g SiO<sub>2</sub> were determined in reference 13h) which resulted in a lower percentage of cell death.<sup>13h</sup>

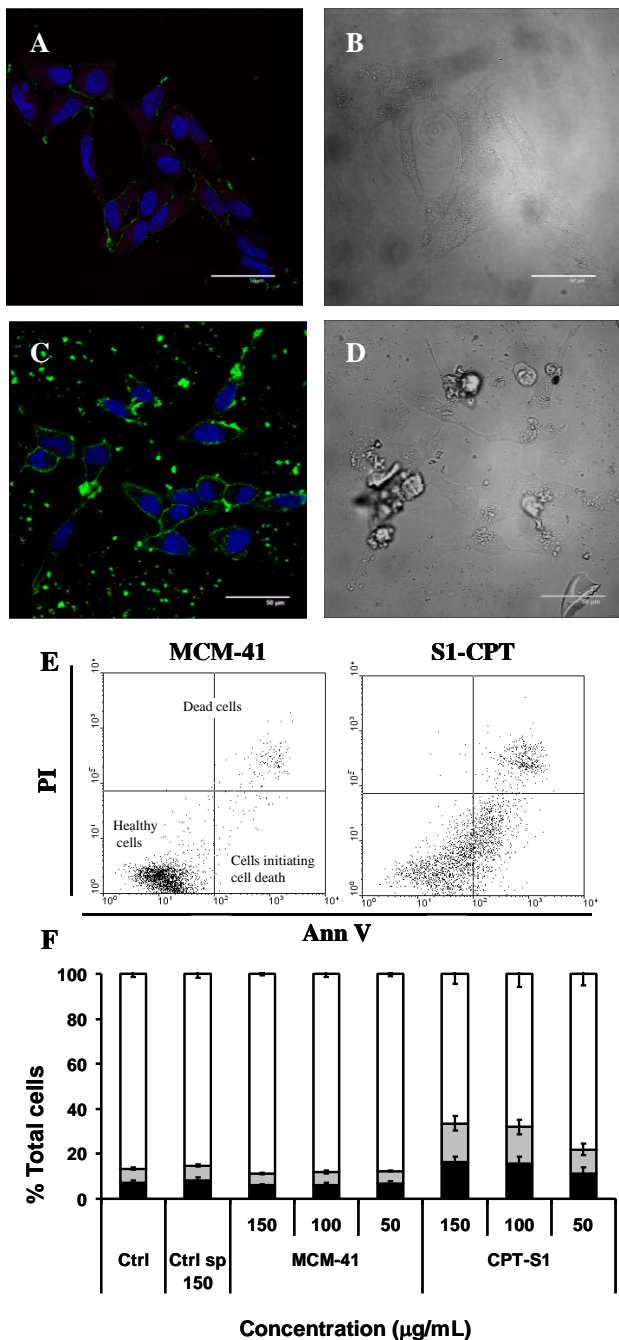


**Fig. 8** S1-CPT cell internalization induces cell death. HeLa cells were treated with control MCM-41 (A, B) or S1-CPT (C, D) at 150 μg/mL, and cells were further incubated for 48 h. MCM-41-treated cells presented normal morphology and remained attached to the plate (A) in the confocal microscopy analysis (B), in which the plasma membrane was stained with WGA Alexa Fluor 647 (green). In contrast, S1-CPT-treated cells presented a phenotype associated with cell death (C) and a cell diffuse pattern of CPT-associated fluorescence (blue) due to CPT release and

subsequent cell death induction. Quantification of cell viability and cell death (E, F) was performed by flow cytometry by means of PI and Ann V stainings, respectively. The percentage of dead cells (black), cells undergoing cell death (gray) and healthy cells (white) are shown after 48 h of treatment. Three independent experiments containing triplicates were performed and the data are reported as (mean ± SE).

Finally, in order to test that CPT release in cells was a consequence of the enzymatic hydrolysis of the gate, controlled release experiences with S1-CPT in a hydrophobic solvent (DMSO) were carried out. These experiences, developed in the absence of enzyme, showed that after 24 hours the amount of CPT release was negligible.

## CONCLUSIONS

The efficiency of a new gated material to deliver its cargo in a controlled manner in the presence of certain enzymes has been proved. In this work, a new “zero-release” system based on the gated nanomaterial S1 has been prepared. This hybrid solid was composed of a nanoparticulated mesoporous scaffolding whose pores were loaded with safranin O dye and whose outer surface was covered with a gluconamide derivative. In the presence of pronase and amidase enzymes, the amide linkage in the gluconamide threads was hydrolyzed with the subsequent safranin O release. This study demonstrates that it is possible to use relatively simple molecules containing enzyme-hydrolyzable groups to design capped materials that can be opened at will. The present work also proves that gluconamide-functionalized nanoparticles are efficiently taken up by tumoral cells. The cellular uptake of nanoparticles probably occurs via endocytosis by targeting them to autolysosomes, where the molecular gate is degraded by lysosomal enzymes and the cargo is released. Finally, the possible application of gluconamide-functionalized nanoparticles as suitable delivery systems in the cells of chemotherapeutic agents, such as CPT, has been demonstrated, and a significant reduction of cell viability has been observed in the cells treated with solid S1-CPT.

## ACKNOWLEDGEMENTS

We thank the Spanish Government (Project MAT2009-14564-C04 and SAF2010-15512) and the Generalitat Valenciana (Project PROMETEO/2009/016 and /2010/005) for support. I. C. thanks the Universitat Politècnica de València for her fellowship. We thank the Confocal Microscopy service of CIPF and the Electronic Microscopy service of UPV for their technical support.

## EXPERIMENTAL SECTION

### Synthesis. General Methods

XRD, TGA, elemental analysis, TEM, <sup>29</sup>Si-NMR and N<sub>2</sub> adsorption-desorption techniques were employed to characterize synthesized materials. Powder X-ray measurements were taken in a Philips D8 Advance diffractometer using Cu Kα radiation. Thermogravimetric analyses were carried out on a TGA/SDTA 851e Mettler Toledo balance using an oxidant atmosphere (air, 80 mL/min) with a heating program consisting of a heating ramp of

10°C per minute from 393 to 1273 K and an isothermal heating step at this temperature for 30 min. TEM images were obtained with a 100 kV Philips CM10 microscope. Dynamic Light Scattering (DLS) studies were conducted at 25 °C using a Malvern Zetasizer Nano ZS equipped with a 4 mW He-Ne solid-state laser operating at 633 nm. Back-scattered light was detected at 173°, and the mean particle diameter was calculated from the quadratic fitting of the correlation function over 12 runs of 10 s duration. All measurements were performed in triplicate on previously sonicated highly dilute aqueous dispersions. N<sub>2</sub> adsorption-desorption isotherms were recorded with a Micromeritics ASAP2010 automated sorption analyzer. Samples were degassed at 70°C in vacuum overnight. Specific surface areas were calculated from the adsorption data in the low pressure range using the BET model. Pore size was determined following the BJH method. <sup>29</sup>Si MAS NMR spectra were recorded using a BrukerAvance 3 instrument 400MHz operating at 400 MHz and a magic angle spinning speed of 10.0 kHz. Fluorescence spectroscopy was carried out with a Felix 32 Analysis, version 1.2 (Build 56) PTI (Photon Technology International). Live cellular internalization studies were performed with a Cytomics FC 500 (Beckman Coulter Inc.) and a confocal Leica microscope was handled with a TCS SP2 system equipped with an acoustic optical beam splitter (AOBS). Cell viability measurements were carried out with a Wallac 1420 workstation.

## Chemicals

Chemicals tetraethylorthosilicate (TEOS), *n*-cetyltrimethylammonium bromide (CTABr), sodium hydroxide (NaOH), safranin O, Pronase from *Streptomyces Griseus*, Peptide Amidase from *Citrus Sinensis* and Esterase from Porcine Liver were provided by Aldrich. N-(3-triethoxysilylpropyl)gluconamide was supplied by Fluorochem. Camptothecin was provided by Sequoia Research Products. D-MEM with L-glutamine, fetal calf serum (FCS), trypan blue solution (0.4%), cell culture grade, trypsin, wheat germ agglutinin (WGA) Alexa Fluor 647, and Hoechst 33342 were acquired from Gibco-Invitrogen. The cell proliferation reagent WST-1 was obtained from Roche Applied Science. Annexin V-FITC (AnnV) was supplied by Immunostep and propidium iodide (PI) came from BD Dickinson. All the products were used as received.

## Synthesis of the Mesoporous MCM-41 Nanoparticles

The MCM-41 mesoporous nanoparticles were synthesized by the following procedure: *n*-cetyltrimethylammoniumbromide (CTABr, 1.00 g, 2.74 mmol) was first dissolved in 480 mL of deionized water. NaOH (aq) (2.00 M, 3.5 mL) was added to the CTABr solution after adjusting the solution temperature to 80°C. TEOS (5 mL, 2.57·10<sup>-2</sup>mol) was then added dropwise to the surfactant solution. The mixture was allowed to stir for 2 h to give a white precipitate. The solid product was centrifuged, and was washed with deionized water and ethanol. Finally, the solid was dried at 60°C (MCM-41 as-synthesized). To prepare the final porous material (MCM-41), the as-synthesized solid was calcined at 550°C using an oxidant atmosphere for 5 h to remove the template phase.

## Synthesis of S1

In a typical synthesis, 0.340 g of templated-free MCM-41 and safranin O dye (0.036 g, 0.1mmol) were suspended in 90 mL of acetonitrile in a round-bottomed flask. To remove the adsorbed water, 10 mL of acetonitrile were distilled in a Dean-Stark set-up. After stirring 24 h at room temperature, an excess of the alkoxysilane derivative N-(3-triethoxysilylpropyl)gluconamide (50% ethanol) (2.86 mL, 3.4 mmol) was added and the final mixture was stirred for 24 h at room temperature. Finally, solid S1 was filtered off, washed with 800 mL of acetonitrile (200mL four times) and dried at 38°C overnight.

## Synthesis of S1-CPT

In a typical synthesis, 0.100 g of templated-free MCM-41 and the a solution of the corresponding amount of camptothecin (56 mg, 0.16 mmol / 5mL ethanol) were suspended in 20 mL of anhydrous acetonitrile. After stirring for 24 h, the corresponding amount of N-(3-triethoxysilylpropyl)gluconamide (50% Ethanol) was added (0.974 mL, 1.15 mmol) and the mixture was stirred for 24 h at room temperature. Finally, solid S1-CPT was filtered. In order to eliminate the non reacted reagents, a suspension of S1-CPT in 200 mL of a chloroform-methanol mixture 3:4 (v/v) was stirred overnight. After filtering the solid, it was dried at vacuum for 1 h and kept in inert atmosphere.

## Dye release studies

In a typical experiment, 2.5 mg of S1 were suspended on 25 mL of water. pH must be previously adjusted to optimum enzyme conditions (pH=7.5 for amidase from *Citrus sinensis*, pH=8.3 for pronase from *Streptomyces griseus*). Then 50 µL of Peptide Amidase from *Citrus sinensis* were added, whereas to evaluate the Pronase and Esterase effects, 3 mg of S1 were suspended on 25 mL of a solution of Pronase from *Streptomyces griseus* or Esterase from *Porcine Liver*, respectively (0.12 mg/mL). These suspensions were used to evaluate the gate-like effect by studying the dye release from the pore voids of the functionalized material. The delivery of safranin O dye from the pore voids to the solution was easily monitored by the fluorescent emission band of the dye centered at 580 nm (excitation at 520 nm).

## Cell Culture Conditions

The HeLa human cervix adenocarcinoma and the MCF-7 human breast adenocarcinoma were purchased from the German Resource Centre for Biological Materials (DSMZ) and were grown in D-MEM and Medium 199 supplemented with 10% of FCS. Cells were maintained at 37°C in an atmosphere of 5% carbon dioxide and 95% air, and they underwent passage twice a week.

## WST-1 Cell Viability Assay

Cells were cultured in sterile 96-well microtiter plates at a seeding density of 2.5x10<sup>3</sup> and 3x10<sup>3</sup> cells/well for HeLa and MCF-7, respectively, and they were allowed to settle for 24 h. S1 in DMSO was added to cells at the final concentrations of 50, 25, 10, and 5 µg/mL. After 23 h, WST-1 (7 µL of a 5 mg/mL solution) was added to each well. Cells were further incubated for 1 h (a total of 24 h of incubation was therefore studied), and absorbance was measured at 450 nm and normalized versus absorbance at 690 nm in a Wallac 1420 workstation.

## Live Confocal Microscopy S1 Cellular Internalization

HeLa and MCF-7 cells were seeded in 24 mm  $\phi$  glass coverslips in 6-well plates at a seeding density of  $5 \cdot 10^4$  cells/well. After 24 h, cells were treated when indicated with **S1** or **S1-CPT** at a final concentration of 50  $\mu\text{g/mL}$ . After 24 h of incubation, cells were stained with 10 ng/mL of Hoechst 33342 and 5 mg/mL WGA Alexa Fluor 647 for 30 min in PBS containing 10% FCS or by keeping the medium for the **S1-DOX** treatments. Slides were visualized under a confocal microscope. Two independent experiments were done and contained triplicates with similar results.

## Cytofluorometry Studies Employing S1

To carry out the cytofluorometry studies, HeLa cells were seeded at  $5 \times 10^4$  cells/well in a 12-well plate. After 24 h, cells were treated with **S1-CPT** at the following concentrations for 48 h: 150, 100 and 50  $\mu\text{g/mL}$ . Then, cells were stained with PI and Ann V according to the manufacturer's protocol (BD Pharmingen). Quantification of PI-positive and AnnV-positive staining was done by the WinMDI program, version 2.9. Three independent experiments were done and contained triplicates with analogous results.

## NOTES AND REFERENCES

<sup>a</sup> Centro de Reconocimiento Molecular y Desarrollo Tecnológico (IDM), Unidad Mixta Universitat Politècnica de València-Universitat de València, Spain.

<sup>b</sup> Departamento de Química, Universitat Politècnica de València, Camino de Vera s/n, 46022, Valencia, Spain. E-mail: [mmaez@qim.upv.es](mailto:mmaez@qim.upv.es)

<sup>c</sup> CIBER de Bioingeniería, Biomateriales y Nanomedicina (CIBER-BBN).

<sup>d</sup> Departamento de Química Orgánica, Facultad de Química, Universitat de València, 46100 Burjassot, Valencia, Spain.

<sup>e</sup> Institut de Ciència dels Materials, Universitat de València, P. O. Box 22085, E-46071, Valencia, Spain.

<sup>f</sup> Centro de Investigación Príncipe Felipe, Laboratorio de Péptidos y Proteínas, Avd. Autopista al Saler, 16, E-46012, Valencia, Spain.

<sup>g</sup> IBV-CSIC, Jaime Roig, 11, E-46010, Valencia, Spain.

- (a) G. A. Ozin, *Adv. Mater.*, 1992, **4**, 612. (b) E. Katz, I. Willner, *Angew. Chem. Int. Ed.*, 2004, **43**, 6042.
- The supramolecular chemistry of organic-inorganic hybrid materials*, (R. Martínez-Máñez, K. Rurack Ed.), 2010, J. Wiley & Sons, Hoboken.
- A. B. Descalzo, R. Martínez-Máñez, F. Sancenón, K. Hoffmann, K. Rurack, *Angew. Chem. Int. Ed.*, 2006, **46**, 5924.
- N. K. Mal, M. Fujiwara, Y. Tanaka, *Nature* 2003, **421**, 350.
- (a) E. Aznar, R. Martínez-Máñez, F. Sancenón, *Expert Opin. Drug Deliv.* 2009, **6**, 643. (b) K. Cotí, M. E. Belowich, M. Liong, M. W. Ambrogio, Y. A. Lau, H. A. Khatib, J. I. Zink, N. M. Khashab, J. F. Stoddart, *Nanoscale*, 2009, **1**, 16.
- (a) R. Casasús, M.D. Marcos, R. Martínez-Máñez, J.V. Ros-Lis, J. Soto, L.A. Villaescusa, P. Amorós, D. Beltrán, C. Guillem, J. Latorre, *J. Am. Chem. Soc.* 2004, **126**, 8612. (b) Q. Yang, S. Wang, P. Fan, L. Wang, Y. Di, K. Lin, F.-S. Xiao, *Chem. Mater.* 2005, **17**, 5999. (c) T. D. Nguyen, K.C.-F. Leung, M. Liong, C. D. Pentecost, J. F. Stoddart, J. I. Zink, *Org. Lett.* 2006, **8**, 3363. (d) C. Park, K. Oh, S. C. Lee, C. Kim, *Angew. Chem., Int. Ed.* 2007, **46**, 1455. (e) R. Casasús, E. Climent, M.D. Marcos, R. Martínez-Máñez, F. Sancenón, J. Soto, P. Amorós, J. Cano, E. Ruiz, *J. Am. Chem. Soc.* 2008, **130**, 1903. (f) N. Knežević, B.G. Trewyn, V.-Y. Lin, *Chem. Eur. J.* 2011, **17**, 3338. (g) R. Liu, P. Liao, J. Liu, P. Feng, *Langmuir* 2011, **27**, 3095. (h) F. Muhammad, M. Guo, W. Qi, F. Sun, A. Wang, Y. Guo, G. Zhu, *J. Am. Chem. Soc.* 2011, **133**, 8778. (i) A. Schlossbauer, C. Dohmen, D. Schaffert, E. Wagner, T. Bein, *Angew. Chem., Int. Ed.* 2011, **50**, 6828. (j) K. Zhou, Y. Wang, X. Huang, K. Luby-Phelps, B.D. Sumer, J. Gao, *Angew. Chem., Int. Ed.* 2011, **50**, 6109.
- (a) Q. Fu, G. V. R. Rao, L. K. Ista, Y. Wu, B. P. Andrzejewski, L. A. Sklar, T. L. Ward, G. P. López, *Adv. Mater.* 2003, **15**, 1262. (b) C.R. Thomas, D.P. Ferris, J.-H. Lee, E. Choi, M.H. Cho, E.S. Kim, J.F. Stoddart, J.-S. Shin, J. Cheon, J.I. Zink, *J. Am. Chem. Soc.* 2010, **132**, 10623. (c) E. Ruiz-Hernández, A. Baeza, M. Vallet-Regí, *ACS Nano* 2011, **5**, 1259. (d) E. Aznar, L. Mondragón, J.V. Ros-Lis, F. Sancenón, M.D. Marcos, R. Martínez-Máñez, J. Soto, E. Pérez-Payá, P. Amorós, *Angew. Chem. Int. Ed.* 2011, **50**, 11172. (e) A. Baeza, E. Guisasaola, E. Ruiz-Hernández, M. Vallet-Regí, *Chem. Mater.* 2012, **24**, 517. (f) J. Croissant, J. I. Zink, *J. Am. Chem. Soc.* 2012, **134**, 7628.
- (a) C.-Y. Lai, B. G. Trewyn, D. M. Jeftinija, K. Jeftinija, S. Xu, S. Jeftinija, V.S.-Y. Lin, *J. Am. Chem. Soc.* 2003, **125**, 4451. (b) R. Hernandez, H.-R. Tseng, J. W. Wong, J. F. Stoddart, J. I. Zink, *J. Am. Chem. Soc.* 2004, **126**, 3370. (c) Y. Zhao, B. G. Trewyn, I. I. Slowing, V.S.-Y. Lin, *J. Am. Chem. Soc.* 2009, **131**, 8398. (d) M. Fujiwara, S. Terashima, Y. Endo, K. Shiokawa, H. Ohue, *Chem. Commun.* 2006, 4635. (e) B. G. Trewyn, S. Giri, I. I. Slowing, V. S.-Y. Lin, *Chem. Commun.* 2007, 3236. (f) R. Liu, Y. Zhang, P. Feng, *J. Am. Chem. Soc.* 2009, **131**, 15128. (g) F. Porta, G.E.M. Lamers, J.I. Zink, A. Kros, *J. Phys. Chem. C* 2011, **13**, 9982. (h) Z. Luo, K. Cai, Y. Hu, L. Zhao, P. Liu, L. Duan, W. Yang, *Angew. Chem., Int. Ed.* 2011, **50**, 640.
- (a) E. Aznar, R. Casasús, B. García-Acosta, M. D. Marcos, R. Martínez-Máñez, F. Sancenón, J. Soto, P. Amorós, *Adv. Mater.* 2007, **19**, 2228. (b) N. G. Liu, Z. Chen, D. R. Dunphy, Y. -B. Jiang, R. A. Assink, C. J. Brinker, *Angew. Chem. Int. Ed.* 2003, **42**, 1731. (c) J. Lu, E. Choi, F. Tamanoi, J. I. Zink, *Small* 2008, **4**, 421. (d) E. Aznar, M.D. Marcos, R. Martínez-Máñez, F. Sancenón, J. Soto, P. Amorós, C. Guillem, *J. Am. Chem. Soc.* 2009, **131**, 6833. (e) X. Yang, X. Liu, Z. Liu, F. Pu, J. Ren, X. Qu, *Adv. Mater.* 2012, **24**, 2890.
- (a) C. Coll, R. Casasús, E. Aznar, M. D. Marcos, R. Martínez-Máñez, F. Sancenón, J. Soto, P. Amorós, *Chem. Commun.* 2007, 1957; (b) E. Aznar, C. Coll, M. D. Marcos, R. Martínez-Máñez, F. Sancenón, J. Soto, P. Amorós, J. Cano, E. Ruiz, *Chem. Eur. J.* 2009, **15**, 6877. (c) E. Climent, M. D. Marcos, R. Martínez-Máñez, F. Sancenón, J. Soto, K. Rurack, P. Amorós, *Angew. Chem., Int. Ed.* 2009, **48**, 8519. (d) I. Candel, A. Bernardos, E. Climent, M. D. Marcos, R. Martínez-Máñez, F. Sancenón, J. Soto, A. Costero, S. Gil, M. Parra, M. Chem. Commun. 2011, **47**, 8313. (e) J. Lee, J. Lee, S. Kim, C.-J. Kim, S. Lee, B. Min, Y. Shin, C. Kim, *Bull. Korean Chem. Soc.* 2011, **32**, 1357.
- See for example: (a) H. Tanga, J. Guoa, Y. Sunb, B. Changa, Q. Renb, W. Yang, *International Journal of Pharmaceutics* 2011, **421**, 388. (b) N. Singh, A. Karambelkar, L. Gu, K. Lin, J.S. Miller, C.S. Chen, M.J. Sailor, S.N. Bhatia, *J. Am. Chem. Soc.*, 2011, **133**, 19582. (c) Q. He, J. Shi, *J. Mater. Chem.*, 2011, **21**, 5845.
- (a) E. Climent, A. Bernardos, R. Martínez-Máñez, A. Maquieira, M. D. Marcos, N. Pastor-Navarro, R. Puchades, F. Sancenón, J. Soto, P. Amorós, *J. Am. Chem. Soc.* 2009, **131**, 14075. (b) E. Climent, R. Martínez-Máñez, F. Sancenón, M. D. Marcos, J. Soto, A. Maquieira, P. Amorós, *Angew. Chem., Int. Ed.* 2010, **49**, 7281. (c) C.-L. Zhu, C.-H. Lu, X.-Y. Song, H.-H. Yang, X.-R. Wang, *J. Am. Chem. Soc.* 2011, **133**, 1278. (d) C. Chen, J. Geng, F. Pu, X. Yang, J. Ren, X. Qu, *Angew. Chem. Int. Ed.* 2011, **50**, 882. (e) Y.L. Choi, J.H. Lee, J. Jaworski, J.H. Jung, *J. Mater. Chem.*, 2012, **22**, 9455.
- (a) K. Patel, S. Angelos, W. R. Dichtel, A. Coskun, Y.-W. Yang, J. I. Zink, J. F. Stoddart, *J. Am. Chem. Soc.* 2008, **130**, 2382. (b) A. Schlossbauer, J. Kecht, J. Bein, *Angew. Chem., Int. Ed.* 2009, **48**, 3092. (c) C. Park, H. Kim, S. Kim, C. Kim, *J. Am. Chem. Soc.* 2009, **131**, 16614. (d) A. Bernardos, L. Mondragón, E. Aznar, M. D. Marcos, R. Martínez-Máñez, F. Sancenón, J. Soto, J. M. Barat, E. Pérez-Payá, C. Guillem, P. Amorós, *ACS Nano* 2010, **4**, 6353. (e) P. D. Thornton, A. Heise, *J. Am. Chem. Soc.* 2010, **132**, 2024. (f) C. Coll, L. Mondragón, R. Martínez-Máñez, F. Sancenón, M. D. Marcos, J. Soto, P. Amorós, E. Pérez-Payá, *Angew. Chem., Int. Ed.* 2011, **50**, 2138. (g) J. Liu, X. Du, X. Zhang, *Chem.-Eur. J.* 2011, **17**, 810. (h) A. Agostini, L. Mondragón, C. Coll, E. Aznar, M.D. Marcos, R. Martínez-Máñez, F. Sancenón, J. Soto, E. Pérez-Payá, P. Amorós, *ChemistryOpen*, 2012, **1**, 17.

- 
- 14 (a) A. Bernardos, E. Aznar, C. Coll, R. Martínez-Máñez, J. M. Barat, M. D. Marcos, F. Sancenón, A. Benito, J. Soto, *Journal of Controlled Release* 2008, **131**, 181; (b) S-H. Cheng, W-N Liao, L-M Chen, C-H. Lee, *J. Mater. Chem.*, 2011, **21**, 7130. (c) Y. Zhu, J. Shi, W. Shen, X. Dong, J. Feng, M. Ruan, Y. Li, *Angew. Chem. Int. Ed.* 2005, **44**, 5083. (d) Y. -F. Zhu, J. -L. Shi, Y. -S. Li, H. -R. Cheng, W. -H. Shen, X. -P. Dong, *Micropor. Mesopor. Mater.* 2005, **85**, 75.
- 15 (a) S-H. Wu, Y. Hung, C-Y. Mou, *Chem Commun* 2011, **47**, 9972. (b) Y.-W. Yang, *Med. Chem. Commun.*, 2011, **2**, 1033. (c) P. Yang, S. Gai, J. Lin, *Chem. Soc. Rev.*, 2012, **41**, 3679.
- 16 (a) S. Cabrera, J. El Haskouri, J. Guillem, J. Latorre, A. Beltrán, D. Beltrán, M. D. Marcos, P. Amorós, *Solid State Sci.* 2000, **2**, 405. (b) D.R. Radu, C-Y. Lai, K. Jęftinija, E.W. Rowe, S. Jęftinija, V.S.Y. Lin, *J. Am. Chem. Soc.* 2004, **126**, 13216.
- 17 N. Gartmann, D. Brühwiler, *Angew. Chem., Int. Ed.* **2009**, *48*, 6354.
- 18 (a) Y. Pommier, *Chem. Rev.*, 2009, **109**, 2894. (b) Q. -Y. Li, Y. -G. Zu, R. -Z. Shi, L. -P. Yao, *Curr. Med. Chem.*, 2006, **13**, 2021.

20

25

30

35

40

45

50

55

60